We found that recruits from infested broods dispersed shorter natal distances (see Methods) than recruits from uninfested broods (mean for broods: infested, 532 ± 57 m; uninfested, 641 ± 44 m; generalized linear model: fleas, $F(1, 67) = 4.52$, $P = 0.04$; controlling for the effects of year, nestling mass and proportion of males (all $P > 0.10$). In contrast to other studies on great tits, which showed greater natal dispersal distances in females[17,18,22], the difference between the sexes was not significant in our study (mean for females, 660 ± 45 m, $N = 53$; mean for males, 547 ± 43, $N = 58$; $F(1, 106) = 1.96$, $P = 0.16$; controlling for year and flea effects). The interaction between flea treatment and sex was not significant ($F(1, 105) = 0.27$, $P = 0.60$), indicating that fleas affected the natal dispersal distance of recruits independently of sex. Fleas could influence natal dispersal distances through an effect on nestling body mass[18,22], hormonal levels in nestlings[24] or through maternal effects[8,12]. These different mechanisms suggest that fleas could have affected the competitive ability of individuals and their cost–benefit balance of dispersal[3,25]. By dispersing shorter distances after growing in flea-infested nests, great tits remain closer to their natal territory where they could be better adapted or show higher tolerance to local parasites[12,26,27]. This effect could be particularly important for females, as they face more frequent contacts with nest-based ectoparasites[12].

Current hypotheses for sex-biased dispersal propose that, in monogamous species with male resource defence like the great tit, males could gain greater benefits from their familiarity with essential local resources by remaining in their natal area[3,10,28]. Our results of a male-biased recruitment in one year, and the interaction between flea treatment and brood size over three years, indicate that benefits of remaining in the natal area could be higher for males growing in large, flea-infested broods. A male-biased dispersal away from our study area from uninfested broods could also potentially explain lower local recruitment of males (Fig. 1). However, such male-biased dispersal would contrast with the female-biased dispersal pattern found in most monogamous birds[3,10,17,28].

To our knowledge, our study shows for the first time that parasite infestations affect host natal dispersal distances and can modify the sex-related probability of fledgling recruitment. Conditional sex-biased dispersal is not predicted by current theoretical models that focus mainly on inbreeding avoidance or local resource competition[2,3,10,25,28]. Key concepts in sex-ratio theory and host–parasite coevolution have been developed by considering the effects of host dispersal[1,4,26,27]. Our results indicate that, in certain organisms, hosts could modify their sex-allocation decisions in response to parasite infestations when parasites modify host sex-biased recruitment and dispersal. □

Methods

Experimental protocol. The study was performed in a population of great tits breeding in a mixed forest near Bern, Switzerland. Breeding pairs were assigned randomly to experimental treatments in each of three breeding seasons (1994–1996). In all three years, parasites were killed in all nests on the day the birds laid their second egg[11–13]. Half the nests in the population were infested by a fixed number of adult fleas from the laying of the second egg or from the start of incubation onwards, whereas the other half were left uninfested. Uninfested nests in 1994 and 1995 were kept free of fleas by heat treatment in a microwave appliance every ten days; in 1996 nests were heat treated only once. Laying date and clutch size did not differ significantly between birds with flea-infested or uninfested nests (Wilcoxon two-sample test: laying date, $Z = -0.09$, $P = 0.93$; clutch size, $Z = 0.38$, $P = 0.71$; $N = 175$ and 168).

Data collection. For each breeding pair we recorded the date when the first egg was laid, clutch size, brood size at hatching, and the number of young fledged. Nestling body mass was measured to the nearest 0.1 g with an electronic balance on days 14 and 16 after hatching. On day 9, all nestlings were ringed with numbered aluminium rings. A local recruit was defined as a fledgling that was recaptured as a first-time breeder in the population until spring 1998. The linear distance between the nest where a young fledged to the nest where it was first re-captured as a breeder was taken as the natal dispersal distance[10]. In 1995,

nestlings of 64 broods were sexed using random amplified polymorphic DNA (RAPD) markers applied to the DNA extracted from blood collected in capillary tubes by venipuncture on 14-day-old nestlings[29]. Mean values are shown $\pm$ standard errors. Analysis was performed in JMP and GLMStat.

1. Hamilton, W. D. Extraordinary sex ratios. *Science* **156,** 477–488 (1967).
2. Hamilton, W. D. & May, R. M. Dispersal in stable habitats. *Nature* **269,** 578–581 (1977).
3. Johnson, M. L. & Gaines, M. S. Evolution of dispersal: theoretical and empirical tests using birds and mammals. *Annu. Rev. Ecol. Syst.* **21,** 449–480 (1990).
4. Herre, E. A. Population structure and the evolution of virulence in nematode parasites of fig wasps. *Science* **259,** 1442–1445 (1993).
5. Clayton, D. H. & Moore, J. *Host–parasite Evolution: General Principles & Avian Models* (Oxford Univ. Press, Oxford, 1997).
6. Richner, H. Host–parasite interactions and life-history evolution. *Zoology* **101,** 333–344 (1998).
7. Brown, C. R. & Brown, M. B. Ectoparasitism as a cause of natal dispersal in cliff swallows. *Ecology* **73,** 1718–1723 (1992).
8. Sorci, G., Massot, M. & Clobert, J. Maternal parasite load increases sprint speed and philopatry in female offspring of the common lizard. *Am. Nat.* **144,** 153–164 (1994).
9. Danchin, E., Boulinier, T. & Massot, M. Conspecific reproductive success and breeding habitat selection: implications for the study of coloniality. *Ecology* **79,** 2415–2428 (1998).
10. Greenwood, P. J. Mating systems, philopatry and dispersal in birds and mammals. *Anim. Behav.* **28,** 1140–1162 (1980).
11. Heeb, P., Werner, I., Richner, H. & Kölliker, M. Horizontal transmission and reproductive rates of hen fleas in great tit nests. *J. Anim. Ecol.* **65,** 474–484 (1996).
12. Heeb, P., Werner, I., Kölliker, M. & Richner, H. Benefits of induced host responses against an ectoparasite. *Proc. R. Soc. Lond.* B **265,** 51–56 (1998).
13. Heeb, P., Kölliker, M. & Richner, H. Bird–ectoparasite interactions, nest humidity and ectoparasite communities. *Ecology* (in the press).
14. Richner, H., Oppliger, A. & Christe, P. Effect of an ectoparasite on reproduction in great tits. *J. Anim. Ecol.* **62,** 703–710 (1993).
15. Tinbergen, J. M. & Boerlijst, M. C. Nestling weight and survival in individual great tits (*Parus major*). *J. Anim. Ecol.* **59,** 1113–1128 (1990).
16. Gebhardt-Heinrich, S. G. & Noordwijk, A. J. V. Nestling growth in the Great tit I. Heritability estimates under different environmental conditions. *J. Evol. Biol.* **3,** 341–362 (1991).
17. Dhondt, A. A. & Hublé, J. Fledging-date and sex in relation to dispersal in young great tits. *Bird study* **15,** 127–134 (1968).
18. Verhulst, S., Perrins, C. M. & Riddington, R. Natal dispersal of great tits in a patchy environment. *Ecology* **78,** 864–872 (1997).
19. Poulin, R. Sexual inequalities in helminth infections: a cost of being a male? *Am. Nat.* **147,** 287–295 (1996).
20. Brown, C. R., Brown, M. B. & Rannala, B. Ectoparasites reduce long-term survival of their avian host. *Proc. R. Soc. Lond.* B **262,** 313–319 (1995).
21. Christe, P., Richner, H. & Oppliger, A. Begging, food provisioning, and nestling competition in great tit brood infested with ectoparasites. *Behav. Ecol.* **7,** 127–131 (1996).
22. Smith, H. G., Källander, H. & Nilsson, J.-Å. The trade-off between offspring number and quality in the great tit *Parus major*. *J. Anim. Ecol.* **58,** 383–402 (1989).
23. Kacelnick, A., Cotton, P. A., Stirling, L. & Wright, J. Food allocation among nestling starlings: sibling competition and the scope of parental choice. *Proc. R. Soc. Lond.* B **259,** 259–263 (1995).
24. Belthoff, J. R. & Dufty, A. M. J. Corticosterone, body condition and locomotor activity: a model for natal dispersal in birds. *Anim. Behav.* **55,** 405–415 (1998).
25. Weatherhead, P. J. & Forbes, M. R. L. Natal philopatry in passerine birds: genetic or ecological influences? *Behav. Ecol.* **5,** 426–433 (1994).
26. Gandon, S., Capowiez, Y., Dubois, Y., Michalakis, Y. & Olivieri, I. Local adaptation and gene-for-gene coevolution in a metapopulation model. *Proc. R. Soc. Lond.* B **263,** 1003–1009 (1996).
27. Kaltz, O. & Shykoff, J. A. Local adaptation in host–parasite systems. *Heredity* **81,** 361–370 (1998).
28. Clarke, A. L., Saether, B.-E. & Roskaft, E. Sex biases in avian dispersal: a reappraisal. *Oikos* **79,** 429–438 (1997).
29. Lessells, C. M. & Mateman, A. C. Sexing birds using random amplified polymorphic DNA (RAPD) markers. *Mol. Ecol.* **7,** 187–195 (1998).
30. Crawley, M. J. *GLIM for Ecologists* (Blackwell Science, Oxford, 1993).

Motion streaks provide a spatial code for motion direction

Wilson S. Geisler

Department of Psychology, University of Texas at Austin, Austin, Texas 78712, USA

Although many neurons in the primary visual cortex (V1) of primates are direction selective[1], they provide ambiguous information about the direction of motion of a stimulus[2,3]. There is evidence that one of the ways in which the visual system resolves this ambiguity is by computing, from the responses of V1 neurons, velocity components in two or more spatial orientations

and then combining these velocity components[2–9]. Here I consider another potential neural mechanism for determining motion direction. When a localized image feature moves fast enough, it should become smeared in space owing to temporal integration in the visual system, creating a spatial signal—a 'motion streak'—oriented in the direction of the motion. The orientation masking and adaptation experiments reported here show that these spatial signals for motion direction exist in the human visual system for feature speeds above about 1 feature width per 100 ms. Computer simulations show that this psychophysical finding is consistent with the known response properties of V1 neurons, and that these spatial signals, when appropriately processed, are sufficient to determine motion direction in natural images.

Neurons in primate area V1 are selective for spatial orientation[1,10]. Thus, a motion streak, even a short one, might produce a maximal response in the population of neurons whose preferred spatial orientation is parallel to the direction of motion. Such a relative maximum response across preferred orientation would be a robust spatial signal for motion direction. On the other hand, most cortical neurons are selective for motion perpendicular to their preferred spatial orientation[1,10]; thus, a maximal response might occur in the population of neurons whose spatial orientation is approximately perpendicular to the direction of motion, at least for some feature speeds.

To determine whether spatial orientation signals for motion direction exist in the human visual system, luminance detection thresholds were measured for moving gaussian dots, as a function of dot size and speed, with dynamic random line masks oriented either parallel or perpendicular to the direction of dot motion. If a moving dot produces larger responses in the population of neurons whose orientation selectivity is parallel to the direction of motion then the parallel mask should be more effective in elevating threshold, because the relevant orientation-selective neurons would be very strongly activated by the mask. The two stimulus conditions are shown in Fig. 1. The target dot moved along the diagonal from the lower left towards the upper right, as indicated by the dashed arrow. A different random sample of line noise was presented in each frame, making the stimulus information for performing the task identical for the two mask orientations. Thresholds were measured for two subjects in a two-interval forced choice task.
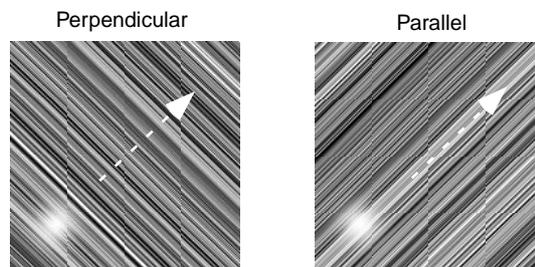
Figure 1 The two stimulus conditions in a masking experiment designed to determine whether the neural mechanisms most responsive to moving dots have their preferred spatial orientations parallel or perpendicular to the direction of motion. Each stimulus presentation consisted of a 25-frame (250-ms) movie. The target dot moved along the diagonal at a given speed, and was added to dynamic random line noise that was oriented either perpendicular or parallel to the direction of dot motion. The luminance threshold for dot detection was measured.

The data for one of the subjects are shown in Fig. 2a–d. Similar results were obtained for the other subject. Each panel shows the data for a different dot size. Within each panel, the vertical axis shows the luminance threshold (cd m^{-2}) for the moving dot, and the horizontal axis shows the speed of the dot motion in degrees per second. (Note that the scale changes from panel to panel.) When the dot was stationary (0° s^{-1}) the thresholds were identical, as expected given the circular symmetry of the dot. This result indicates that the differences in the effectiveness of the two mask orientations are not due to astigmatism or other optical factors. As the speed of movement of the dot increased, the thresholds remained the same until a critical dot speed was reached, beyond which the parallel mask became more effective. To estimate this critical speed, a four-parameter descriptive function was fitted to the data (solid curves in Fig. 2a–d). The descriptive function was specified by coordinates defining the right end-point of the horizontal line segment, and by a pair of slope parameters for the two rising segments of the data. Figure 2e shows the estimated critical speed (the end-point of the horizontal line segment) for the two subjects.

Apparently, whenever its speed exceeds about 1 dot width per 100 ms (dashed line), a moving dot produces a greater response in the population of neurons whose receptive fields are oriented
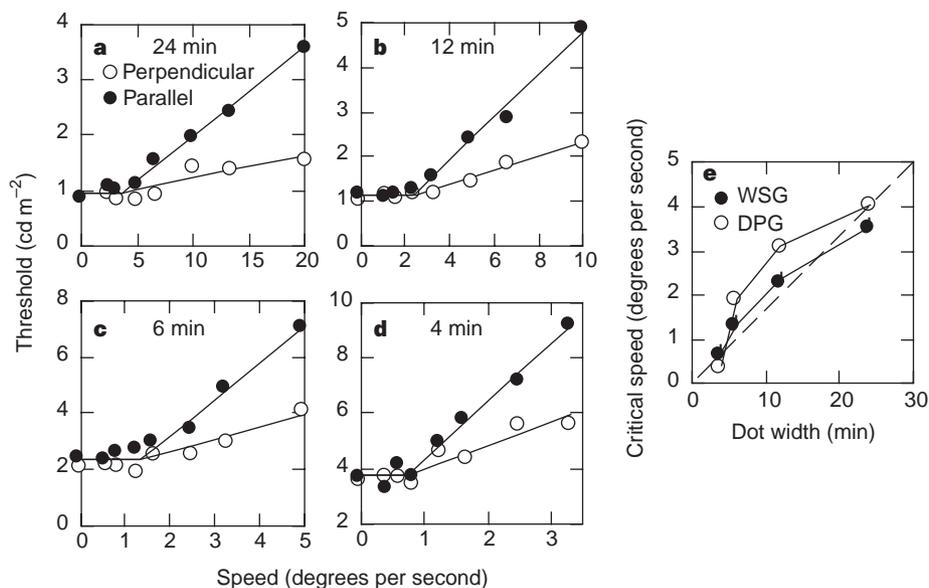
Figure 2 Results of forced-choice detection experiment. **a–d**, Luminance detection thresholds for target dots of 4, 6, 12 and 24 arcmin diameter, as a function of dot speed, for subject W.S.G. Solid symbols: line mask parallel to the direction of motion; open symbols: line mask perpendicular to the direction of motion. Below a critical speed there is no effect of mask orientation; above that speed the parallel mask is more effective. **e**, Critical speed as function of dot width for the two subjects. Dashed line indicates 1 dot width per 100 ms.

parallel to the direction of motion. There seems to be no speed at which a greater response occurs in the population of neurons whose receptive fields are oriented perpendicular to the direction of motion. A second experiment, measuring detection threshold as a function of the orientation difference between the mask and the moving dot, showed that orientation differences between 0° (parallel) and 90° (perpendicular) produce intermediate levels of threshold elevation. Thus, the experimental results indicate that there is a robust and stable spatial orientation signal for motion direction in the visual system for a wide range of speeds, down to less than $1° s^{-1}$ for the smallest dot size.

I used computer simulations to determine whether these psychophysical results are consistent with what would be expected from the responses of V1 neurons. The responses of cortical 'simple cells' and 'complex cells' were simulated using the mean values of the tuning characteristics for V1 neurons reported elsewhere (see Methods)[11]. The preferred spatial frequency of the simulated neurons was set to the value that produced the greatest response to a 6-min dot (9 cycles per degree). Figure 3a shows, as a function of the speed of the moving dot, the peak response for motion parallel to the preferred spatial orientation divided by the peak response for motion perpendicular to the preferred spatial orientation. The solid circles show this response ratio for a dot trajectory passing through the centre of the receptive field of a non-direction-selective cell. Note that the psychophysically measured critical speed for this dot size (indicated by the vertical arrow) is near the speed at which the response ratio begins to exceed 1.0. The triangles show the

response ratio for a direction-selective cell whose preferred direction corresponds to the direction of dot motion. For this cell the response ratio is much less than 1.0 at low speeds. However, the response ratio of the summed responses of two direction-selective neurons with opposite motion-direction preferences is similar to the response ratio of the non-direction-selective cell. Furthermore, essentially identical results were obtained for simple and complex cells. Thus, the simulations indicate that the psychophysical results are consistent with the population response expected to be obtained by pooling across V1 neurons with the same preferred spatial orientation.

Although the masking experiments indicate that a spatial orientation signal for motion direction exists in the human visual system, two important concerns remain. The first is that motion streaks provide ambiguous information about the direction of motion. A detected streak could be the result of a moving feature, or it could be a static image contour. Even if it is the result of a moving feature, the direction in which the feature moved along the orientation of the streak is uncertain. The second concern is whether the spatial orientation signals would actually be very useful for determining motion direction in natural images, because natural images generally contain an extremely complex mixture of extended contours and localized features.

These concerns were addressed by considering the performance of the spatial motion-direction sensor shown in Fig. 3b. The proposed sensor combines multiplicatively an oriented 'non-direction-selective cell' with a perpendicularly oriented 'direction-selective (motion
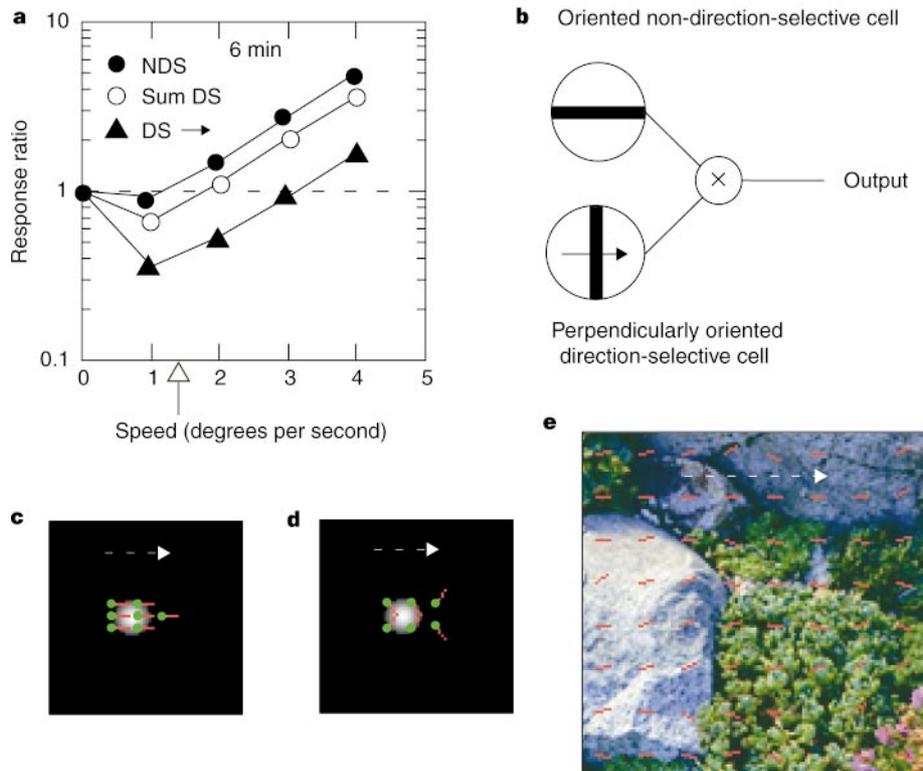
Figure 3 Neural simulations. **a**, Computed responses of typical cortical neurons in primate V1 for a 6-min dot moving parallel or perpendicular to the preferred spatial orientation of the neuron. The ratio of the response in the parallel direction to that in the perpendicular direction is plotted as a function of dot speed. Results are shown for a non-direction-selective cell (NDS), a cell that prefers motion to the right (DS →) and the sum of the responses of a cell that prefers motion to the right with one that prefers motion to the left (sum DS). **b**, A possible neural sensor for determining motion direction from motion streaks. An oriented non-direction-selective cell (or population of cells) is combined multiplicatively with a perpendicularly oriented direction-selective cell (or population of cells). **c**, Responses of a field of spatial motion direction sensors (of all preferred

orientations) to a 6-min Gaussian dot moving at $4° s^{-1}$ in the direction of the arrow. For each location indicated by a green dot, the red line segment shows the orientation of the motion sensor which produced the largest response. **d**, Responses of a field of direction-selective cells alone. The line segments are drawn perpendicular to the orientation of the cells which produced the largest response. **e**, Responses of a field of spatial motion sensors to a 1° × 1° natural image moving in the direction of the arrow. The orientations of the red line segments indicate the estimated direction of motion in each 7.5-min square block. The direction estimates are given by $\hat{\theta} = \arctan[\Sigma R_i \sin\theta_i / \Sigma R_i \cos\theta_i]$, where θ_i is the preferred spatial orientation of the ith sensor at the given location, and R_i is the response of the sensor.

opponent[12]) cell'. For this sensor, localized features moving to the right in the preferred orientation of the non-direction-selective cell will produce a large response, whereas stationary features or features moving to the left will produce no response. The simulations described below show that the sensor produces a more accurate and stable signal for the motion direction of localized features than does the typical direction-selective cell in V1.

Two versions of the sensor were tested. In the first version, the response of the non-direction-selective cell was directly multiplied by the response of the direction-selective cell. The second version was designed to evaluate the usefulness of the spatial motion signals by using as little information as possible from the direction-selective cells. In this case, the response of the direction-selective cell was applied as a simple logical operator: if the response was positive, indicating motion in one general direction (for example, 0–180°), the non-direction-selective cell response was multiplied by one; otherwise, it was multiplied by zero. The two versions gave similar results. The performance of the second version is shown here.

Figure 3c shows the response of a dense array of motion-direction sensors to a 6-min gaussian dot moving from left to right at $4°\,s^{-1}$. The sensor array consisted of 36 sensors (one for every 10° orientation) centred on each image pixel. Each red line segment indicates the preferred orientation of the sensor that gave the largest response at the spatial location indicated by the green dot. The sensors that gave the largest responses corresponded to the true direction of motion. This behaviour holds over a wide range of dot velocities. For comparison, Fig. 3d shows the response of a similar array of direction-selective cells. At this dot speed, the cells that gave the largest response corresponded to either 60° or −60° from the true direction of motion. In general, as dot speed increases, the largest responses correspond to directions that are increasingly far from the true direction of motion.

Figure 3e shows the motion direction estimated at each location in a $1° \times 1°$ natural image moving at $4°\,s^{-1}$ to the right. The natural image movie was created by sliding (in effect) a larger image past a 128×128-pixel viewing aperture. Although the motion direction is not estimated accurately everywhere in the image, the estimates are generally good. Similar results were obtained for other natural images. Thus, it seems safe to conclude that there is almost always useful motion-direction information encoded by spatial mechanisms in the visual cortex once critical speed is exceeded.

The psychophysical results and the simulations show that moving image features produce robust spatial orientation signals in the human visual system, even at low speeds, and that these signals contain useful information about motion direction. Although it is unlikely that this information would be ignored by the brain, the results so far do not prove that motion streaks are used in determining motion direction. Some preliminary evidence that they are used for this purpose was obtained in an orientation adaptation experiment. Two subjects adjusted the apparent direction of a moving 12-min dot (on a dark background) until it appeared to move vertically, after adaptation to a 4 cycles per degree grating oriented either 10° to the left, 10° to the right, or vertically. The measurements for left and right adaption were combined and subtracted from the vertical baseline measurements. Figure 4a shows the results for dot speeds of $2.5°\,s^{-1}$ and $10°\,s^{-1}$, which should produce weak and strong motion streaks, respectively (Fig. 2b). If motion streaks are being used to determine motion direction then orientation adaptation should have a stronger effect on the apparent motion direction of the faster moving dot. This is what was found. An alternative explanation for the result might be based upon the fact that the slower-moving dot covered a smaller total distance. However, this was ruled out with measurements for static dots located at the end points of the motion path. As can be seen in Fig. 4b, the shift is approximately the same for both dot separations.

There is evidence that the visual system contains mechanisms for
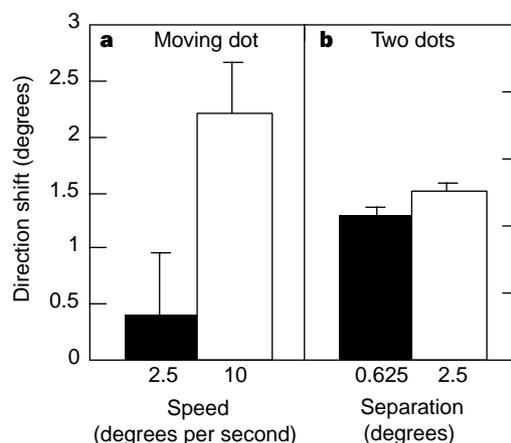
Figure 4 Results of tilt after-effect experiment. **a**, Effect of adaptation to a grating tilted 10° from vertical on the perceived direction of a 12-min dot moving vertically, at one of two speeds. **b**, Effect of adaptation on the perceived orientation of a static pair of dots oriented vertically, at one to of two spatial separations. The vertical axis represents the shift in motion direction or orientation required to cancel the adaptation effect.

suppressing the apparent blur due to motion[13–16]. Such mechanisms are thought to be valuable for preserving the apparent spatial structure of objects across different speeds (for example, maintaining shape constancy). By contrast, my data show that motion blur produces substantial responses in orientation-selective mechanisms, even at low speeds, and that these spatial signals are used for encoding moving objects. These two aspects of motion blur are not incompatible; the spatial motion signals in area V1 may be amplified in areas of the brain responsible for encoding motion, but suppressed in areas of the brain responsible for shape and object representation. This hypothesis is consistent with recent demonstrations that blur discrimination performance is uncorrelated with the reduced apparent blur of moving stimuli[17].

In conclusion, the psychophysical experiments and physiological analyses reported here indicate that, in addition to estimating motion direction by combining velocity components, the human visual system may also estimate motion direction by performing a spatial analysis of motion streaks. An advantage of this scheme is that the two approaches for estimating motion direction are complementary: as speed increases, estimates of velocity components become less reliable, while the estimates of the orientation of motion streaks becomes more reliable. □

Methods

Experiment. The subjects were two experienced psychophysical observers with normal acuity. The stimuli were displayed on a Philips monitor (Model 201B) run at a frame rate of 100 Hz and a spatial resolution of 640×480, using only the green gun ($x = 0.295$, $y = 0.580$). At the viewing distance of 236 cm, the 480×480-pixel random mask was $6.8° \times 6.8°$ in visual angle. Each frame of the random mask consisted of lines one pixel wide that were randomly assigned a luminance of either $0.8\,cd\,m^{-2}$ or $1.92\,cd\,m^{-2}$. For subject D.P.G., the random line masks were diagonal, as in Fig. 1; for subject W.S.G., who was run first, the random line masks were vertical and horizontal. (Diagonal masks were used for D.P.G. because pretesting revealed a slightly greater effect of vertical maskers when the dots were stationary.) The dot target was a radially symmetrical two-dimensional gaussian and was added to the random line mask. In the plots, the dot width is defined as four times the standard deviation of the gaussian.

Four-point psychometric functions were measured with a two-interval blocked forced choice procedure, using the method of constant stimuli. A different dynamic random mask appeared in each interval and the target dot was added to one of the two intervals at random. The durations of the mask and the dot were both 250 ms. The amplitude of the dot was ramped on in the first

50 ms and off in the last 50 ms by a raised cosine function. The two presentation intervals were separated by 500 ms, and the trials were separated by 2,300 ms. Feedback was provided on each trial. Five blocks of 30 trials were run for each psychometric function. To allow for adaptation to the random line masks and to provide some practice, the amplitude of the dot in the first and second blocks was made the same, and the responses from the first block were discarded. The data points in Fig. 2 represent the average of two thresholds estimated from psychometric functions measured a number of days apart. The order of conditions in the repeated session was opposite to that in the first session, to minimize fatigue/practice artefacts.

Simulations. The simulations involved computing the responses of model neurons to movies consisting of 32 frames of 128×128 pixel images, representing a movie duration of 0.25 s and an image area of $1° \times 1°$. Generally, there were 36 model neurons (one for every $10°$ orientation) centred on each image pixel location. In different simulations, the model neurons were 'simple cells', 'complex cells', 'motion opponent cells' or the proposed 'motion-direction sensors'. Most of the receptive field characteristics of the model neurons were fixed at the average values reported for the monkey[11]: orientation bandwidth, $40°$; spatial frequency bandwidth, 1.5 octaves; preferred temporal frequency, 8 Hz; temporal frequency bandwidth, 2.5 octaves; nonlinear response exponent, 2. The preferred spatial frequency of the model neurons was kept at 9 cycles per degree, and the direction-selectivity index ($1 - $ non-preferred/preferred) of the direction-selective cells at 0.9. (The bandwidths and direction selectivity refer to the effective values after applying the response exponent.)

The methods of computing responses were similar to those described in refs 5 and 12. The convolutions for each orientation were computed separately using Fourier methods. The component shapes of the spatial transfer function were a gaussian function on a log axis (the so-called log Gabor function) for one spatial direction, and a gaussian function centred on the origin for the other spatial direction. The component shape of the temporal transfer function was the transfer function of a difference-of-gammas function. (Component shapes corresponding to the Hilbert transforms of the log Gabor and difference-of-gammas functions were also used.) The degree of direction selectivity was controlled by combining these components with an appropriate weighting factor[5,12].

After multiplication of the transformed movie by the transfer function, the result was inverse transformed. To obtain 'simple cell' responses, the log Gabor component of the transfer function was set to cosine phase; the inverse transform was half-wave rectified and squared. To obtain 'complex cell' responses, the inverse transform was computed separately with the log Gabor component in cosine phase and in sine phase; the cosine-phase and sine-phase responses were then squared and summed[5,12]. 'Motion opponent cell' responses were obtained by differencing the responses of complex cells having opposite preferred directions of motion and the same preferred spatial orientation[5,12].

1. Hubel, D. H. & Wiesel, T. N. Receptive fields and functional architecture of monkey striate cortex. *J. Physiol. (Lond.)* **195**, 215–243 (1968).
2. Marr, D. & Ullman, S. Direction selectivity and its use in early visual processing. *Proc. R. Soc. Lond. B* **212**, 151–180 (1981).
3. Adelson, E. H. & Movshon, J. A. Phenomenal coherence of moving visual patterns. *Nature* **300**, 523–525 (1982).
4. Albright, T. D. Direction and orientation selectivity of neurons in visual area MT of the macaque. *J. Neurophysiol.* **52**, 1106–1130 (1984).
5. Watson, A. B. & Ahumada, A. J. Model of human visual-motion sensing. *J. Opt. Soc. Am. A* **2**, 322–342 (1985).
6. Simoncelli, E. P. & Heeger, D. J. A model of neuronal responses in visual area MT. *Vision Res.* **38**, 743–761 (1998).
7. Smith, A. T. & Snowden, R. J. (eds) *Visual Detection of Motion* (Academic, London, 1994).
8. Derrington, A. & Suero, M. Motion of complex patterns is computed from the perceived motions of their components. *Vision Res.* **31**, 139–149 (1991).
9. Stone, L. S., Watson, A. B. & Mulligan, J. B. Effect of contrast on the perceived direction of a moving plaid. *Vision Res.* **30**, 1049–1067 (1990).
10. De Valois, R. L., Yund, E. W. & Hepler, N. The orientation and direction selectivity of cells in macaque visual cortex. *Vision Res.* **22**, 531–544 (1982).
11. Geisler, W. S. & Albrecht, D. G. Visual cortex neurons in monkeys and cats: Detection, discrimination, and identification. *Vis. Neurosci.* **14**, 897–919 (1997).
12. Adelson, E. H. & Bergen, J. R. Spatiotemporal energy models for the perception of motion. *J. Opt. Soc. Am.* **2**, 284–299 (1985).
13. Anderson, C. H. & Van Essen, D. C. Blur into focus. *Nature* **343**, 419–420 (1990).
14. Morgan, M. J. & Benton, S. Motion-deblurring in human vision. *Nature* **340**, 385–386 (1989).
15. Ramachandran, V. S., Madhusudhan Rao, V. & Vidyasagar, T. R. Sharpness constancy during movement perception. *Perception* **3**, 97–98 (1974).
16. Burr, D. Motion smear. *Nature* **284**, 164–165 (1980).
17. Burr, D. C. & Morgan, M. J. Motion deblurring in human vision. *Proc. R. Soc. Lond. B* **264**, 431–436 (1997).

Mox2 is a component of the genetic hierarchy controlling limb muscle development

Baljinder S. Mankoo*, Nina S. Collins*, Peter Ashby†‖, Elena Grigorieva*, Larysa H. Pevny‡‖, Albert Candia§‖, Christopher V. E. Wright§, Peter W. J. Rigby† & Vassilis Pachnis*

Divisions of *Developmental Neurobiology, †Eukaryotic Molecular Genetics and ‡ Developmental Genetics, MRC National Institute for Medical Research, The Ridgeway, Mill Hill, London NW7 1AA, UK
§ Vanderbilt Medical School, B2317A MCN, 1161 21st Avenue South, Nashville, Tennessee 37232-2175, USA

The skeletal muscles of the limbs develop from myogenic progenitors that originate in the paraxial mesoderm and migrate into the limb-bud mesenchyme[1]. Among the genes known to be important for muscle development in mammalian embryos are those encoding the basic helix-loop-helix (bHLH) myogenic regulatory factors (MRFs; *MyoD, Myf5, myogenin* and *MRF4*)[2–4] and *Pax3*, a paired-type homeobox gene that is critical for the development of limb musculature[5–7]. *Mox1* and *Mox2* are closely related homeobox genes that are expressed in overlapping patterns in the paraxial mesoderm and its derivatives[8,9]. Here we show that mice homozygous for a null mutation of *Mox2* have a developmental defect of the limb musculature, characterized by an overall reduction in muscle mass and elimination of specific muscles. *Mox2* is not needed for the migration of myogenic precursors into the limb bud, but it is essential for normal appendicular muscle formation and for the normal regulation of myogenic genes, as demonstrated by the downregulation of *Pax3* and *Myf5* but not *MyoD* in *Mox2*-deficient limb buds. Our findings show that the MOX2 homeoprotein is an important regulator of vertebrate limb myogenesis.

Mox1 and *Mox2* are co-expressed in the epithelial somites of mouse embryos[8,9] (Fig. 1a, c). In differentiating somites, both genes continue to be expressed in the sclerotome, but the dermomyotome expresses only *Mox1*[8,9] (Fig. 1b, d, i). Limb buds also show differential regulation of *Mox* genes, in which *Mox2* (but not *Mox1*) messenger RNA was detected in a pattern consistent with expression in the migrating myoblasts and their derivative muscles[9] (Fig. 1e–h). This was further demonstrated by double labelling with immunohistochemistry for MOX2 and *in situ* hybridization histochemistry for *Pax3*, a gene that is expressed in limb buds, specifically in the dermomyotome-derived myoblasts[5–7,10]. *Pax3* and *Mox2* were co-expressed in most migrating myoblasts as soon as they de-epithelialized from the dermomyotome and entered the limb-bud mesenchyme (Fig. 1i–j). To identify further the *Mox2*-expressing cells in limb buds, we analysed the expression of *Mox2* in homozygous *Splotch* (*Sp*) embryos, in which a mutation at the *Pax3* locus prevents the migration of myogenic precursors from their site of origin in the paraxial mesoderm into the limb buds[5,6,10]. *Mox2* transcripts, which are seen in scattered cells in the proximal region of forelimbs and hindlimbs of embryonic day 10.5 (E10.5) +/+ or +/*Sp* embryos, were absent from the limbs of their *Sp/Sp* littermates (Fig. 1k–l and data not shown). These data show that, in the

‖ Present addresses: Wellcome Trust Building, University of Dundee, WTB/MSI Complex, Dow Street, Dundee DD1 5EH, UK (P.A.); Developmental Genetics Programme, Krebs Institute, University of Sheffield, Sheffield S10 2TN, UK (L.H.P.); Department of Developmental Biology, Stanford University, Stanford, California 94305, USA (A.C.).